Nuclear hyperpolarization of ^{3}He by magnetized plasmas

A. Maul,[1] P. Blümler,[1] P.-J. Nacher,[2] E. Otten,[1] G. Tastevin,[2] and W. Heil[1,*]

[1]*Institute of Physics, University of Mainz, 55128 Mainz, Germany*

[2]*Laboratoire Kastler Brossel, ENS-PSL University, Centre National de la Recherche Scientifique, Sorbonne Université, Collège de France, 24 rue Lhomond, 75005 Paris, France*

(Received 20 June 2018; published 5 December 2018)

We describe a method, referred to as PAMP (polarization of atoms in a magnetized plasma), that allows hyperpolarization of ^{3}He nuclear spins at high magnetic field solely by excitation of a rf gas discharge. A magnetized plasma is obtained when the mean free path of the free electrons is much larger than their gyration radius in the rf gas discharge. Investigations of PAMP are carried out in the 1–15-mbar pressure range with rf excitation around 100 MHz. Quantitative NMR measurements at 4.7 T and room temperature show that, for different cell sizes and gas densities, ^{3}He nuclear polarizations in the 1 to 9% range are achieved (i.e., larger than the Boltzmann equilibrium spin polarization of the free electrons). A description involving alignment-to-orientation conversion in the excited $2\,^3P$ state is proposed. The PAMP method appears as a very attractive alternative to established laser polarization techniques (spin exchange or metastability exchange optical pumping). Application to ^{3}He nuclear magnetometry with a relative precision of 10^{-12} is demonstrated.

DOI: 10.1103/PhysRevA.98.063405

I. INTRODUCTION

Metastability exchange optical pumping (MEOP) is an efficient method to create hyperpolarization in ^{3}He, i.e., nuclear orientation which is far beyond the equilibrium polarization that can be reached at the lowest temperatures and in the highest magnetic fields available at the moment. The method, developed by Colegrove, Schearer, and Walters [1], is an extension of ordinary optical pumping [2,3] where the light-induced atomic orientation is directly created in the ground state. In ^{3}He MEOP operates on the excited metastable $2\,^3S_1$ state produced in a plasma discharge sustained in the gas. MEOP is usually performed in low magnetic field up to a few millitesla and efficiently operates at low pressure of order 1 mbar where nuclear polarization of up to 90% has been reported [4]. The hyperfine interaction provides the physical mechanism for the polarization transfer from the polarized light to the ^{3}He nuclei. Polarization is ultimately transferred to the ground state through metastability exchange collisions. MEOP can still be used up to several tesla and yields high polarizations even at elevated gas pressures, in spite of large hyperfine decoupling at high magnetic fields. In a recent paper [5] the physics and technology of producing large quantities of highly spin-polarized ^{3}He nuclei using MEOP are reviewed.

There is a rather large domain of possible applications of hyperpolarized (HP) ^{3}He ranging from polarized targets for nuclear and particle physics [6,7], neutron spin filters [8–10], and contrast agents in lung magnetic resonance imaging [11,12] to measurements and monitoring of magnetic fields [13–15]. For the latter we have demonstrated that a ^{3}He nuclear magnetometer is able to measure high magnetic fields ($B > 0.1$ T) with a relative accuracy of better than 10^{-12} [13]. Our approach is based on the measurement of the free induction decay (FID) of HP-^{3}He following a resonant rf pulse excitation (i.e., a pulsed NMR experiment). The measurement sensitivity can be attributed to the long coherent spin precession time T_2^* being of the order of minutes which is achieved for spherical sample cells in the regime of "motional narrowing" where the disturbing influence of field inhomogeneities is strongly suppressed.

Performing such MEOP experiments routinely in our laboratory we observed that NMR signals were detected even when the pumping laser was turned off accidentally. Although they were much weaker than those obtained with laser optical pumping these unexpected signals were evidence of considerable hyperpolarization (large out-of-equilibrium nuclear polarization) that arises from the discharge in the absence of laser light (signals decayed and vanished if the discharge was turned off as well).

As it turned out, Carver and coworkers [16,17] had also observed discharge-induced nuclear polarization of ground-state ^{3}He atoms in rf discharges already in the late 1960s. The reported nuclear polarization, obtained at 3.1-amagat gas density in a 1-T field, was about four times higher than the Boltzmann equilibrium polarization and had a positive or negative sign depending on the type of rf excitation (intermittent or continous discharge). The authors tentatively attributed this phenomenon to Overhauser polarization by distinct saturated species present in the plasma. Later, McCall and Carver [17] reported further investigations at lower number density (2.7–46.6-mbar ^{3}He gas pressure) for field strengths up to 0.8 T and various types of gas excitation. They reported nuclear polarization up to 0.06% at 0.1 T, and a change in sign from positive to negative as field strength was increased (with a zero crossing at around 0.45 T). They put emphasis on experimental features that would suggest that the metastable triplet atoms are involved both in the transfer of nuclear

*Corresponding author: wheil@uni-mainz.de

polarization to the ^{3}He ground state and in the polarization enhancement process.

Our studies are performed at higher field strength (a few tesla), and an Overhauer-like mechanism cannot account for our results, because the polarization levels we measure (up to almost 10%) significantly exceed even those of thermally polarized electrons or paramagnetic atoms. Since production of HP ^{3}He gas without lasers will be of great practical advantage, particularly for use in magnetometry [13] and because the origin of the observed effect seems not yet clearly established, we have investigated the influence of the operating conditions on achieved polarizations and buildup rates. Here, we report on NMR measurements performed on spherical ^{3}He gas samples at 4.7 T for different cell volumes, filling pressures, and rf excitation levels. The experimental setup is described in Sec. II. The collected data are presented in Sec. III. A demonstration of application to high-field magnetometry is discussed in Sec. IV. The details of the determination of the absolute polarization are described in Appendix A, and the explanation of the effect via an alignment-to-orientation conversion (AOC) mechanism can be found in Appendix B. We suggest to use the acronym PAMP, for polarization of atoms in a magnetized plasma, to describe the method that allows one to obtain nuclear hyperpolarization solely from a gas discharge in which the mean free path of the electrons is large compared to their cyclotron radius.

II. EXPERIMENTAL SETUP FOR MEOP AND PAMP

Figure 1 shows a schematic drawing and photograph of the experimental setup. The sample consists of a spherical glass cell which is filled with a few millibars of pure ^{3}He. Several cells with inner diameter $\emptyset_{\mathrm{ID}}$ were used ($8 < \emptyset_{\mathrm{ID}} < 20$ mm), all blown from standard Pyrex glass with a wall thickness of $\sim$1 mm. Each cell was successively cleaned with Mucasol[1] and rinsed with distilled water, evacuated, baked out, and finally filled with the desired ^{3}He pressure before it was sealed off by a torch. Cells were mounted inside a NMR-probe coil [see Fig. 1(b)] and placed inside a superconducting magnet at 4.7 T (homogeneity $\sim$1 ppm/cm). The remaining sealing stem of the cells was always oriented perpendicular to the direction of the magnetic field in order to reduce field gradients across the sample volume originating from magnetic susceptibility mismatch [13].

For investigation of either MEOP or PAMP the setup allows (1) hyperpolarization with polarized laser light incident on a ^{3}He plasma (i.e., MEOP) and (2) PAMP experiments without laser excitation [here the beam is simply blocked while the plasma is kept burning; see Fig. 1(a)]. The plasma is generated by a discharge coil, which was a solenoid in the case of MEOP and the laser was shone on the sample through its inner core. Otherwise the discharge coil was tightly wound onto the glass cell. In both cases, the discharge coil axis was oriented parallel to the magnetic field.

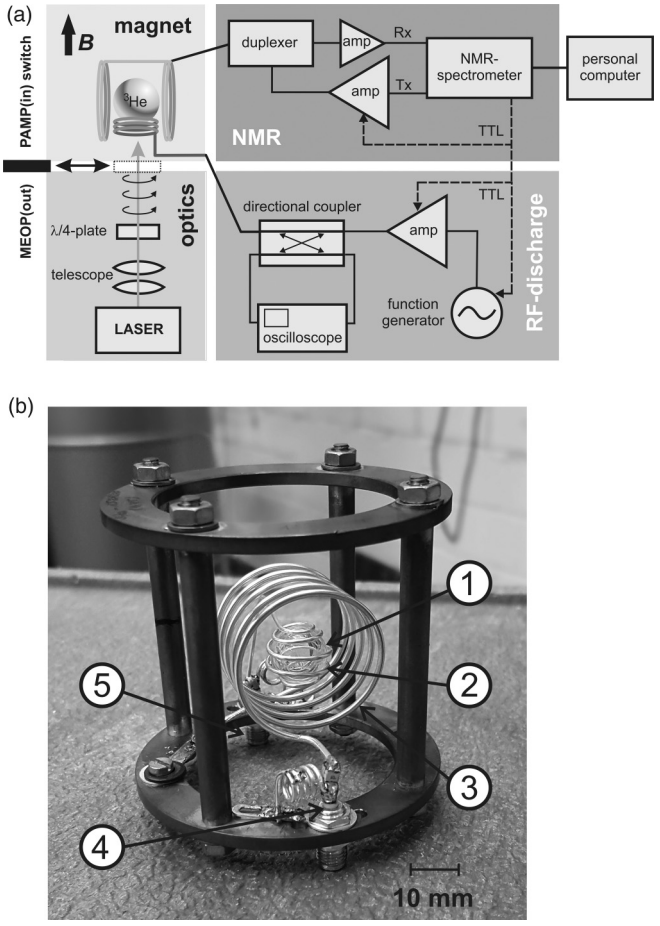

FIG. 1. (a) Schematic drawing of the experimental setup. The sample is immersed in a strong and homogeneous magnetic field, $B = 4.7$ T. The depicted probe configuration, used for MEOP, includes a solenoidal discharge coil (holding the cell) and a Helmholtz NMR coil pair. It is connected to three experimental parts: (*optics*) circularly polarized light of 1083 nm provided by a 2W Yb-doped fiber laser[2], (*RF discharge*) a discharge circuit for plasma ignition, and (*NMR*) NMR excitation and detection. The NMR spectrometer controls and synchronizes the entire setup via a data connection to a PC. When the laser (*optics*) beam is blocked the MEOP experiment is switched to a PAMP experiment, as sketched in the upper left. (b) Photograph showing the probe configuration for PAMP: (1) Spherical glass sample with ^{3}He, (2) discharge coil wound on the gas container, (3) NMR solenoidal coil, (4) NMR-coil connector, and (5) discharge coil connector.

The discharge coil was part of a serial *LC* circuit carefully tuned and matched prior to each experiment. Coil dimensions and available rf capacitors typically yield resonance frequencies in the 100–120-MHz range produced by a sine generator, amplified, and fed into the *LC* circuit. Matching conditions (minimal reflected rf signal, purely resistive impedance $R = 50\ \Omega$) were constantly monitored using a bidirectional high-power rf coupler [see Fig. 1(a)]. Here we pragmatically report the rf excitation level in terms of the effective power, p_{eff}, which is dissipated in the discharge circuit and helium cell.

[1]Mucasol is a trademark of Merz GmbH & Co. KG: universal cleaning agent for labware and instruments made of glass.

[2]Keopsys, 2 Rue Paul Sabatier, 22300 Lannion, France

To this aim, we use the measurements of forward, U_f, and reflected, U_r, rf voltages to infer

$$p_{\text{eff}} = (U_f - U_r)^2/2R. \quad (1)$$

An infrared photodiode (sensitivity range: 850–1070 nm) located next to the ^{3}He cell monitors some amount of fluorescent light emitted by the discharge. In the present paper, the photodiode signals were principally used as indicators of the discharge brightness which in contrast to p_{eff} better reflect the actual plasma intensity.

NMR excitation and detection was performed with either a Helmholtz (for MEOP experiments) or a solenoidal rf coil (PAMP), tuned to the Larmor frequency of ^{3}He, f_L($f_L = 152.26$ MHz), and oriented perpendicular to the magnetic field. The entire experiment was controlled by a KEA spectrometer[3] that managed the NMR excitation and signal acquisition as well as the gating of the discharge via transistor-transistor-logic (TTL) control of the rf amplifier. Typical NMR-acquisition parameters were flip angle 90°, pulse length 40–50 μs, and dwell times 0.1–1 ms. If not mentioned otherwise, the FID signal from a single NMR excitation was recorded. The initial amplitude, S, of the FID signal was used as a measure of the magnitude of the nuclear polarization. Absolute polarization values were inferred from the NMR sensitivity factor derived from calibration measurements (Appendix A).

For the MEOP-PAMP comparison reported in Sec. III A, a standard MEOP setup was used, similar to the one described in [13]. It includes a 1083-nm laser source for excitation of the $2\,^3S$-$2\,^3P$ transition as well as a circular polarizer and optical elements for light beam control.

The buildup[4] of the nuclear polarization signal $S(t)$ in the ^{3}He plasma detected via the monitored FID signal may generally be described by a single exponential growth rate, Γ, and an asymptotic value, S_∞, such that

$$S(t) = S_\infty[1 - \exp(-\Gamma t)]. \quad (2)$$

III. DISCHARGE POLARIZATION RESULTS

This section gives a quantitative survey of the various dependencies of the gas discharge polarization in PAMP experiments on several parameter settings. Additionally, it begins with the determination of the orientation of the ^{3}He nuclear spins in a dedicated MEOP-PAMP comparison.

A. Sign of the ^{3}He nuclear polarization

The nuclear polarization, P, is defined as

$$P = \frac{N_+ - N_-}{N_+ + N_-}, \quad (3)$$

where N_+ and N_- are the population numbers for the two nuclear spin states, $m_I = \pm 1/2$ of ^{3}He ($I = 1/2$). Unambiguous determination of the orientation of the nuclear spins produced by the rf excitation for PAMP can be obtained by comparison with that achieved by MEOP. This comparison is particularly easy to perform at 4.7 T thanks to large Zeeman energy splittings between magnetic eigenstates and strong differences in resonance line positions in the 1083-nm absorption spectrum of ^{3}He (see Fig. 1 in [18]).

We have selected two strong absorption lines, the so-called f_4^+- and f_2^+-transition lines of ^{3}He, which are accessible within the 120-GHz broad tuning range of our laser [19] and are well resolved at room temperature (the atomic Doppler full width at half maximum, 2 GHz, is small compared to the $f_4^+ - f_2^+$ line splitting of 9.1 GHz). They both belong to the 1083-nm absorption spectrum of ^{3}He for the *same* circular light polarization (σ^+) but yield nuclear spin polarization with *opposite* signs [20]: the f_2^+ transition depletes N_- (and hence creates $P > 0$) and the opposite is true for pumping via the f_4^+ line.

Two experiments have been performed in which ^{3}He gas was maintained under constant rf excitation (except during NMR measurements), and the laser, tuned to one resonance line (f_2^+ or f_4^+), was shone onto the sample for a 20-s period of MEOP, then blocked. The results are shown in Fig. 2. In both cases, the NMR signal rapidly increases during the MEOP period, towards a finite asymptotic value, and starts to decay when the laser is blocked. For f_4^+ pumping [Fig. 2(a)] the signal amplitude monotonically decays towards a finite and smaller asymptotic value. For f_2^+ pumping [Fig. 2(b)] the signal amplitude decays, reaches a null value, then grows towards an (also smaller) asymptotic value. The change in sign is indicated by the kink at the point of zero polarization. The fact that the asymptotic NMR signals diverge by about a factor of 2 is to be attributed to the difference in rf discharge powers used during both examinations. From these observations, we conclude that PAMP induces *negative* ^{3}He nuclear polarization at 4.7 T, as does f_4^+ pumping.

B. Dependence on discharge power

By increasing the applied rf power [p_{eff}, as obtained with Eq. (1)] a strong growth of the PAMP-induced NMR signal was observed. It was also noticed that not all power must have been transferred to the plasma. First of all the electrical losses cause heating of the tank circuit at higher currents. This will then detune the tank circuit driving it out of the resonance conditions. Besides that, the power dissipation in capacitively (or inductively) coupled rf discharges has to be considered; this has been studied, e.g., in [21]. The properties of capacitively and/or inductively coupled discharges are strongly influenced by the discharge intrinsic structure. It consists of a positive columnlike discharge volume, the glow space or "bulk," and two specific interaction regions between the bulk and the dielectric walls in front of the field-supplying electrodes, the "sheaths."[5] The power dissipation in the sheath

[3] Magritek, Unit 3, 6 Hurring Place, Newlands, Wellington 6037, New Zealand.

[4] The signal amplitude of the nuclear polarization was probed at different times in consecutively repeated experiments each starting with initial polarization $P(t = 0) = 0$.

[5] A sheath layer is several Debye lengths thick. The value of this length, $\lambda_D = \sqrt{\varepsilon_0 k_B T_e/(n_e e^2)}$, depends on various characteristics of the plasma (e.g., electron temperature T_e and density n_e). In a weakly ionized gas discharge, $\lambda_D \sim 0.15$ mm.

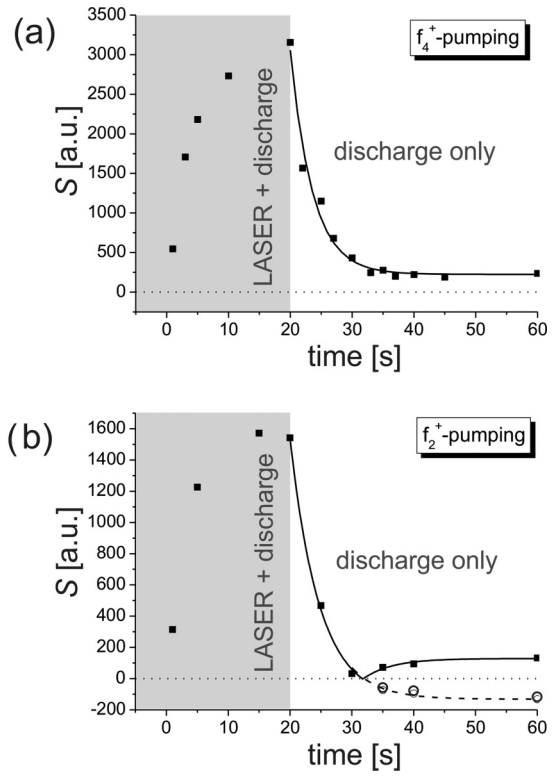

FIG. 2. Development of the NMR signal of ^{3}He in an experiment where polarization was built up by MEOP in the first 20 s (gray shaded area); thereafter the laser was blocked while the rf discharge was kept burning. The magnitude of the nuclear polarization (black solid symbols) was probed at different times in consecutively repeated experiments. For this the discharge was switched off and a NMR experiment was performed. (a), (b) Polarizing with the laser tuned (a) to the f_4^+ line (yielding $P < 0$) and (b) to the f_2^+ line (yielding $P > 0$). Both experiments were done at 4.7 T on a spherical sample (inner diameter: 8 mm, pressure ∼1 mbar). The full symbols represent the measured initial amplitudes of the NMR signal while the open symbols in (b) correspond to the opposite (mirrored) values. The curves describing the ^{3}He discharge relaxation after blocking the laser are monoexponential decays. Reliable NMR calibration (see Appendix A) was not available for these specific experiments, therefore actual polarization values cannot be given. However, with similar cells we routinely got a polarization of ∼25% by MEOP in a 1.5-T field [13]. From that we can make an educated guess that PAMP (discharge only) produces a nuclear polarization of ∼2%.

regions [22][6] is one of the main loss processes and generally increases with increasing rf current. Thus, the characterization of rf discharge conditions by the transmitted rf power measurements is weakly relevant since only a small fraction of the total measured rf power is related to the electron heating process which governs the electron energy probability function (EEPF) in the luminous bulk plasma [23]. Therefore the luminous intensity of the bulk plasma was monitored by means of a photodiode. Figure 3(a) shows the dependence of the plasma light intensity versus the effective discharge power which can be described by an exponential approach towards a saturation value and has been used as a reference for the actual plasma intensity.

To investigate the influence of discharge power on the PAMP polarization buildup, NMR measurements were made about 1 s after the discharge was stopped. The rf power, p_{eff}, was varied in consecutive runs from ∼1 to 50 W. Figure 3(b) shows its influence on the respective buildup curves of the observed ^{3}He NMR signals, i.e., a general increase of both polarization buildup rate (Γ) and saturation polarization (S_∞) with increasing rf power. The situation becomes clearer [see Fig. 3(c)] when these curves are fitted with Eq. (2) and the fit parameters S_∞ and Γ are plotted versus the plasma intensity as measured by the photodiode in Fig. 3(a). This removes the strong nonlinearity between the applied electric power and the intensity of the induced plasma, the bulk plasma. Of course, there are insufficiencies in using the U_{D} signal to describe the bulk plasma: self-absorption, emitted spectrum changes as the discharge power is increased, finite spectral range of photodiodes, etc. The obvious stronger increase of the S_∞ and Γ values (outliners) at the highest discharge power [see Fig. 3(c)] may be attributed to a not-one-to-one assignment of the actual discharge power in the bulk plasma as measured by the photodiode.

C. Influence of sample volume and ^{3}He gas pressure

Polarization influencing parameters which can easily be varied are sample size and filling pressure. Therefore, three different types of spherical sample cells of average size $\emptyset_{\mathrm{ID}} =$ 8.2, 10.8, and 19.2 mm were filled with four different ^{3}He pressures [$p_{\mathrm{He}} = 1.0(5)$, 5.0(5), 10.0(5), and 15.0(5) mbars], i.e., a total of 12 cells were prepared. PAMP measurements have been performed at discharge powers p_{eff} in the 30–50-W range. While the discharge coils were always snugly fitted to the sample size, the NMR-detection circuit was not altered to ensure comparable NMR sensitivity. Like in Fig. 3(b) the amplitudes of the observed ^{3}He NMR signals were recorded as a function of the discharge duration. Using the monoexponential saturation law from Eq. (2) the fit parameters S_∞ and Γ were extracted. In order to reference the measured NMR signal S_∞ to the corresponding polarization value P_∞, a NMR signal calibration was performed with thermally polarized ^{3}He samples. The procedure is described in Appendix A. By use of Eq. (A4) the corresponding magnitude of polarization values $|P_\infty|$ could then be deduced. They are compiled and plotted as a function of the cell filling pressure in Fig. 4. In all cases the discharge-induced nuclear polarization of ^{3}He generally exceeds the thermal limit of electronic Boltzmann polarization which is $P_{\mathrm{th}}^{\mathrm{e}^-} = -1.08\%$ at 4.7 T and room temperature (293 K).

Looking at the characteristic polarization buildup rates, Γ (see Fig. 5), there is no uniform picture in the various dependencies on pressure and sample volume except for a general decrease with pressure. Given a constant rf power in the bulk

[6]Typical electron temperatures T_{e} in a glow discharge plasma are in the range of 1–10 eV; ion temperature and neutral gas temperature are relatively low, around 0.03 eV. However, the energy of ions bombarding the substrate can exceed T_{e}. This is due to the net positive space charge in the plasma sheath leading to a potential profile that falls sharply to the local substrate potential near the boundary.

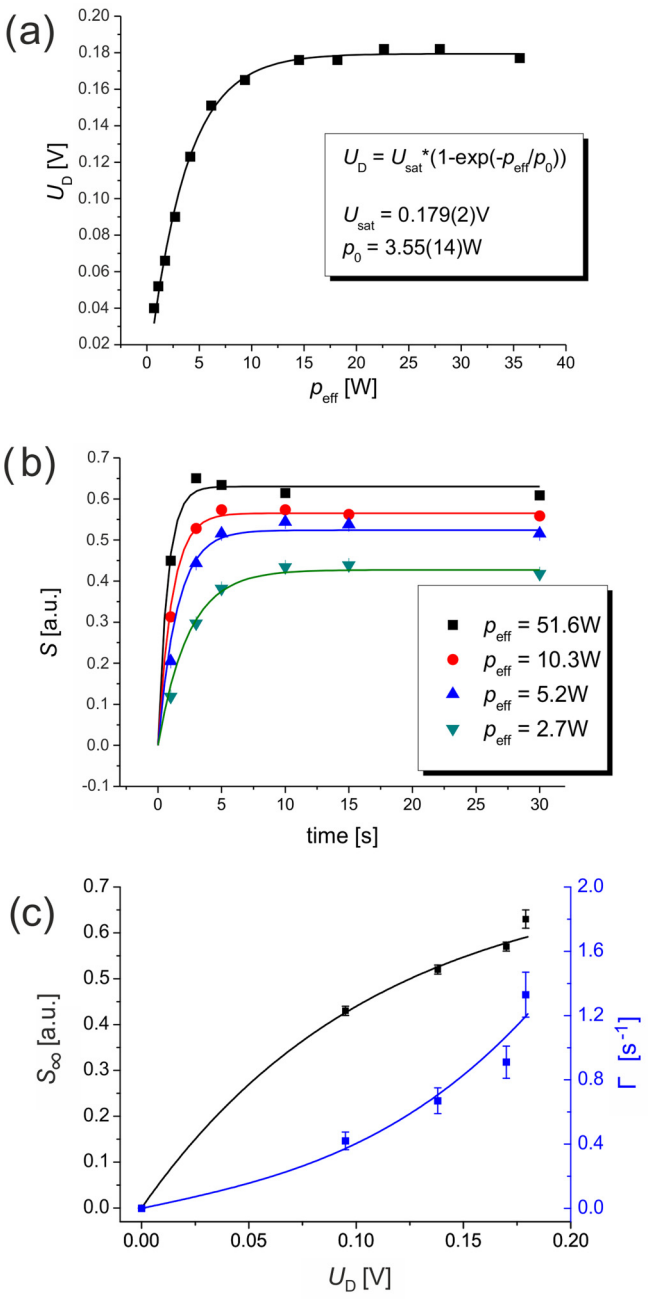

FIG. 3. (a) Photodiode voltage signal, U_D, vs the electrical power p_{eff} applied to the discharge coil. The black curve represents an exponential fit. (b) PAMP ^{3}He NMR signals versus discharge duration for four different discharge powers (2.7, 5.2, 10.3, and 51.6 W, from bottom to top). The solid lines are fits of Eq. (2) to the data. This graph is meant to show results from a spherical cell ($\varnothing_{ID} = 10.8$ mm and p_{He} of about 1 mbar) yielding relatively high polarization buildup rates ($\Gamma \approx 1\ s^{-1}$). Much smaller Γ's were observed for other sample diameters and pressures (see Sec. III.C). (c) Fit parameters obtained for the data in (b). S_∞(black squares) and Γ (blue dots) are plotted against the photodiode signal U_D, using the fit in (a). When discharge is off ($U_D = 0$), no polarization signal is observed ($S_\infty = 0$) and Γ essentially reduces to the negligible contribution from the wall relaxation rate [hence, we set $\Gamma(U_D = 0) \approx 0$]. The blue solid line is a third-order polynominal fit to the measured Γ data. The lines are essentially a guide for the eyes since no explicit model is involved.

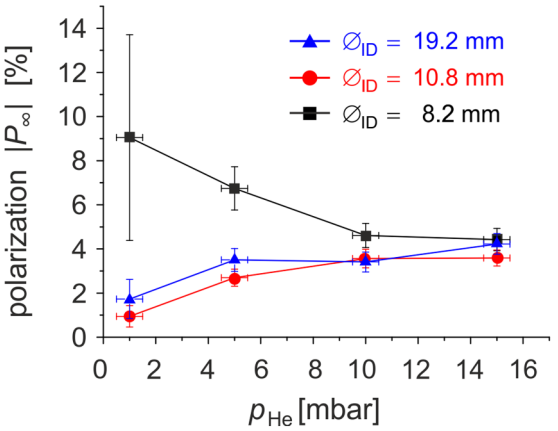

FIG. 4. Measurements of absolute polarization $|P_\infty|$ produced by PAMP in various spherical samples of different ^{3}He pressures and three different cell diameters: black squares, $\varnothing_{ID} = 8.2$ mm; red dots, $\varnothing_{ID} = 10.8$ mm; and blue triangles, $\varnothing_{ID} = 19.2$ mm. The absolute polarization was determined by the procedure described in Appendix A. The increase of the error bars towards lower gas pressures essentially results from the overall pressure uncertainty of ±0.5 mbar [see Eq. (A4)]. The measurements were conducted in a magnetic field of $B = 4.7$ T.

discharge plasma one might expect Γ to decrease with increasing sample volume and pressure according to $\Gamma \propto 1/(p_{He}V)$. A general decrease towards higher filling pressures can be observed particularly at the sample cells with the largest size ($\varnothing_{ID} = 19.2$ mm), but the expected volume dependency is hardly pronounced. In one particular measurement, namely, with the cell $\varnothing_{ID} = 10.8$ mm, we have observed a giant rise of Γ by almost a factor 100 in lowering the pressure from 5 mbars to 1 mbar (see Fig. 5). This is associated with a drop in nuclear polarization, too. From the plasma light intensity which was also recorded we can deduce a strong dependence on the fine tuning of the rf matching circuit which maximizes the effective power delivered to the plasma. That may explain to some extent an observed resonancelike increase of the

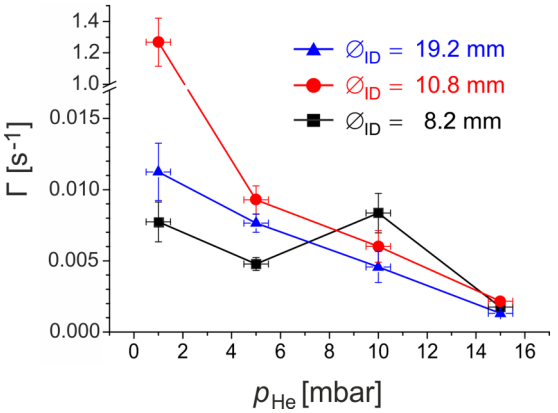

FIG. 5. Measurements of polarization buildup rate Γ for various gas pressures and sample diameters $\varnothing_{ID}$ (black squares, 8.2 mm; red dots, 10.8 mm; blue triangles, 19.2 mm). The notably larger (by a factor 100) buildup rate Γ measured in the $\varnothing_{ID} = 10.8$ mm cell is presumably due to the onset of a different discharge mode.

polarization buildup rate for that particular case. But also abrupt changes in the EEPF shape with a corresponding drop in the effective electron temperature and a rapid increase of the plasma density are well known in the rf discharge literature [23]. This goes along with the transition from the α to the γ mode at given gas pressures and rf discharge strength.[7] In the α mode (Joule heating), electron and ion motion in the plasma body are collisionally dominated by the plasma's spatial distribution controlled by ambipolar diffusion and collisional electron heating is the main rf power dissipation process. In the γ mode, secondary electrons[8] (born at the rf electrodes due to ion bombardment) and other electrons (due to electron avalanche or ion ionization in the sheaths) accelerate in the rf sheaths towards the plasma where they perform intensive ionization and excitation.

At strong magnetic fields, the magnetic confinement (see Appendix B) drastically changes the ionization balance and the plasma's radial distribution (particularly inhomogeneous at higher gas pressures, for $p_{\mathrm{He}} > 30$ mbars [24]). In that case, the light-emitting plasma is generally nonuniform and mostly located close to the walls of the cell. Moreover, the nature of the rf discharge is also deeply modified by cell geometry (cell size, thickness of dielectric walls, etc.) and rf excitation frequency [22,25].

In summary, these rather complex interrelationships do not allow us to explain on a quantitative basis the experimentally observed dependencies of $|P_\infty|$ and Γ on sample volume and ^{3}He gas density (see Figs. 4 and 5). They certainly would require a deeper investigation on capacitively or inductively driven rf discharges, in particular the monitoring of the evolution of the spatial density distribution of the $2\,^3S$ metastable states and the role of the EEPF integral-based quantities as the plasma density n_{e} and the effective electron temperature T_{e} (see Appendix B). However, in view of the application of PAMP to high-precision magnetometry (which requires small spherical cells) such an investigation seems both difficult and unnecessary.

IV. PAMP-BASED MAGNETOMETRY

Since a potentially important use of the PAMP effect is to design simple and extremely sensitive magnetometers, we now demonstrate this application with two experiments performed with 1-mbar gas samples. The first sample was contained in a $\emptyset_{\mathrm{ID}} = 8.2$ mm glass sphere with a wall thickness of $\sim$1 mm, and a short stem, selected among the set of ^{3}He cells used for the NMR measurements reported in Sec. III. The ^{3}He sample has been polarized by rf excitation with $p_{\mathrm{eff}} = 39$ W up to saturation polarization.[9] Figure 6(a) shows the recorded FID signal following a single 90° NMR pulse. The high signal-noise ratio (R_{SN}) of 1050 (referenced to a bandwidth, f_{BW}, of 1 Hz) clearly demonstrates the efficiency of polarizing

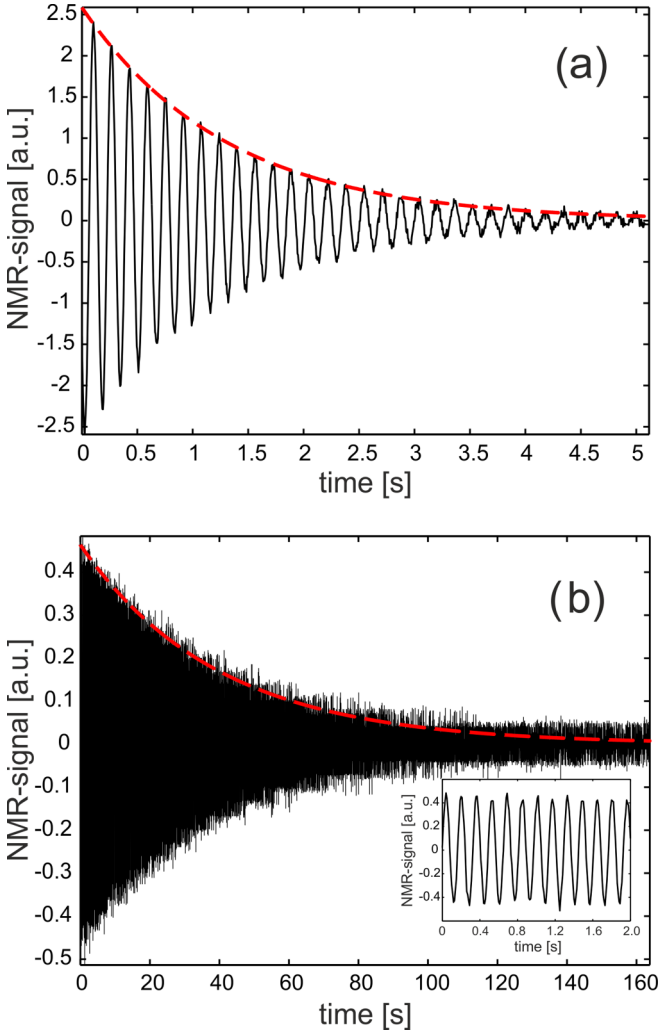

FIG. 6. FID signal (real part only) measured at low beat frequency $f_b = f_{\mathrm{L}} - 152.26$ MHz from two samples polarized via PAMP at 4.7 T. (a) Cell with stem and 1-mm-thick walls ($\emptyset_{\mathrm{ID}} = 8.2$ mm, $p_{\mathrm{He}} = 1$ mbar); 1k data were acquired with a dwell time of 5 ms. (b) Sample of high sphericity but 2-mm-thick walls ($\emptyset_{\mathrm{ID}} = 8.0$ mm, $p_{\mathrm{He}} \sim 1$ mbar [26]); 16k data were sampled with a dwell time of 10 ms. Inset: The first 2 s of the signal for direct comparison with (a). The red dashed line indicates a monoexponential fit to the data in order to determine T_2^* which is 1.28 s for (a) and 39.7 s for (b). Note the different scales of the time axes.

the ^{3}He via PAMP. In this experiment, a pronounced stem significantly shortened the signal lifetime ($T_2^* = 1.3$ s) as a result of a nonspherical susceptibilty distribution that causes static field inhomogeneities [13]. The second sample was contained in a quartz cell of almost perfect sphericity and similar diameter ($\emptyset_{\mathrm{ID}} = 8.0$ mm) designed and used for ^{3}He magnetometry [26]. In contast to the first sample cell, the FID signal, shown in Fig. 6(b), had a much longer lifetime ($T_2^* = 40$ s). The lower R_{SN} of the FID recording ($\sim$100 at $f_{\mathrm{BW}} = 1$ Hz) measured with this cell may be attributed to the relatively thick dielectric container wall of 2 mm hampering the rf excitation of the gas. Moreover, it was recognized that the gas discharge showed a slightly different color which is an indication of gas contamination stemming from impurities

[7] In [23] transitions can occur in the pressure region $\Delta p < 5$ mbars depending on the current density of the rf gas discharge.

[8] In an electrodeless discharge, this should not be relevant.

[9] The characteristic polarization buildup time was $\tau_{\mathrm{pol}} \approx 130$ s. In the case of the spherical quartz cell (second sample) we measured $\tau_{\mathrm{pol}} \approx 3$ s.

desorbed from the walls during the discharge process. Gas impurities quench the density of metastable ^{3}He atoms and thus may reduce the PAMP efficiency (see Appendix B).

Following the data treatment presented in [13], the magnetometers' sensitivity across the respective T_2^* time interval is $\delta B/B = 2.5 \times 10^{-12}$ for Fig. 6(a) and $\delta B/B = 1.1 \times 10^{-12}$ for Fig. 6(b). Here two very different data result in a very similar sensitivity because the sensitivity scales $\propto R_{SN} \cdot (T_2^*)^{3/2}$. A longer T_2^* provides an obvious advantage in monitoring and controlling a field. Therefore, further improvement of the PAMP sensitivity requires thin walled cells of perfect sphericity and presumably very high gas purity even at the elevated cell temperatures.

V. DISCUSSION AND OUTLOOK

The main objective of the present paper is to report, first, on the observation of ^{3}He hyperpolarization solely due to plasma excitation (PAMP) in the presence of a high magnetic field (4.7 T) and, second, on the measurement of ground-state nuclear spin polarization a few times higher than the thermal Boltzmann limit of free electrons. The PAMP mechanism is described in terms of an alignment-to-orientation conversion in helium (see Appendix B).

Complementary tests have been made to provide a quick overview of the dynamic range of PAMP. Using available high-field magnets and NMR systems, we have checked that significant NMR signals could be obtained at various field strengths and temperatures. Under each of such conditions no attempt was made to accurately quantify or optimize the observed signal. We operated in 1.5-, 7-, and 11.7-T magnets using a blown spherical cell with $\emptyset_{ID} \approx 20$ mm and 1.2-mbar filling pressure. Relying on local information for the NMR calibration, the evaluated nuclear polarization values fall within the $0.1 < |P_\infty| < 1\%$ range.

PAMP tests were performed at 77 K and around 10 K in a 4-T magnet (used for Penning trap experiments in Heidelberg) using a 1.5-mbar ^{3}He cell of similar size. The actual temperature of the gas was not measured. Moderate rf power (<3 W) was used to limit thermal load. NMR amplitudes could not be calibrated or quantitatively compared. But as we measured R_{SN} of the FID signal we reached 670:1 at 77 K and 90:1 at 10 K in a bandwidth of 1 Hz (for comparison see Fig. 6).

Further tests of PAMP have been performed in a ^{4}He-rich isotopic mixture and in pure ^{129}Xe gas. They were both motivated by prior MEOP experiments. The addition of ^{4}He in MEOP cells is known to yield higher nuclear ^{3}He polarizations and shorter buildup rates, provided that optical pumping selectively operates on ^{4}He metastable state atoms [27]. The higher probability of light absorption by the even isotope contributes to make this indirect pumping method more efficient in many situations (in spite of the needed transfer of orientation to the metastable state ^{3}He atoms, by metastability exchange collisions between the optically pumped metastable state ^{4}He atoms and ground-state ^{3}He atoms, as a first step). Similarly, addition of ^{4}He might be advantageous for PAMP if metastable state atoms play a key role in the polarization process. This is apparently not the case as tested with a $\emptyset_{ID} \approx 20$ mm gas cell filled with 3.0 mbars of ^{3}He and 7.2 mbars of ^{4}He at 4.7 T. However, we cannot exclude that a higher density of impurities in the test sample of isotopic gas mixture may have limited PAMP efficiency.

No PAMP signal has been detected in the ^{129}Xe test cell ($\emptyset_{ID} \approx 20$ mm), filled with low pressure ^{129}Xe gas around 2 mbars, at room temperature and 4.7 T. We believe that NMR sensitivity would have allowed detection of nuclear polarization if it were comparable to (or moderately smaller than) that achieved in ^{3}He. The absence of sizable signal is in line with the negative result of the attempts to use MEOP for hyperpolarization of xenon: optical polarization of ^{129}Xe metastable state atoms is successful, but ground-state nuclear polarization systematically fails to be detected [28,29].

In the context of precision magnetometry, small cells are used as field probes. Detailed quantitative experimental proof of the underlying physics and analysis of the effects of PAMP within such field probes seem very difficult and are not planned. Some technical improvements will still be performed. Already in its present status precision magnetometry obviously benefits from the PAMP effect, because the experiment can be compacted and miniaturized (thanks to dispensable optical components). A comprehensive study of the field dependence of PAMP efficiency would be very interesting. From Eq. (B4) we may expect that the efficiency will drop significantly when the electron mean free path λ approaches the gyration radius r_c. However, from the work of Carver and coworkers [16,17] we expect this drop to occur below 0.1 T. The limit to PAMP efficiency at high magnetic fields will probably be set by full (fine and hyperfine) magnetic decoupling in the excited states [30].

In conclusion, our experimental findings seem very encouraging but obviously call for further work. Systematic investigations are needed to establish the full potential of PAMP. Theoretical work is also highly desirable and would facilitate optimization and exploitation of the method.

ACKNOWLEDGMENTS

We are thankful to Rainer Jera for providing innumerous glass cells on demand. Financial support by the Deutsche Forschungsgemeinschaft under Grant No. He2308/16-1 and by the cluster of excellence PRISMA "Precision Physics, Fundamental Interactions and Structure of Matter" is also greatly acknowledged.

APPENDIX A: NMR SIGNAL CALIBRATION WITH THERMALLY POLARIZED ^{3}He SAMPLES

In order to determine the absolute polarization of ^{3}He from NMR data it is possible to reference the measured amplitudes versus the known thermal nuclear polarization:

$$P_{th} = \tanh \frac{\hbar \gamma B}{2 k_B T}, \tag{A1}$$

where $\hbar$ is the Planck constant, γ the gyromagnetic ratio of ^{3}He ($\gamma_{He}/2\pi = -32.434$ MHz/T [31]), and k_B is the Boltzmann constant. It is small (10^{-5} at room temperature and 4.7 T, typically; see Table I), hence high gas density and fast signal averaging (of $\bar{n} \approx 1000$ FID signals) are needed for accurate reference measurements. Sealed glass spheres of different volumes, filled with relatively high ^{3}He pressures

TABLE I. Parameter values for the four O_2-doped ^{3}He gas samples used for NMR signal calibration.

Sample	No. 1	No. 2	No. 3	No. 4
V (mm^3)	711(58)	1830(220)	2631(280)	3547(343)
$\emptyset_{ID}$ (mm)	11.08(30)	15.18(60)	17.12(60)	18.92(60)
p_{He} (mbar)	495.0(5)	495.0(5)	650.0(5)	495.0(5)
p_{O2} (mbar)	≈3000	≈3000	≈3000	≈3000
$10^5 \times P_{th}(= 293\,\mathrm{K}, B = 4.7\,\mathrm{T})$	–1.25(2)	–1.25(2)	–1.25(2)	–1.25(2)
$\langle S_{th}\rangle$(a.u.) ($\bar{n} \approx 1000$, typically)	0.479(1)	1.245(4)	2.054(10)	2.170(13)

(typically 0.5 bar), were prepared. Since the bulk longitudinal nuclear relaxation time T_1 can amount to hours in pure ^{3}He, it needs to be shortened for fast signal averaging. Relaxation can be much faster if molecular oxygen is added, but about 3 bars of O_2 are required to obtain T_1 as short as 1 s [32]. Therefore, the thermal decomposition of an inorganic peroxide was used to release O_2 after sealing. We used strontium peroxide which decomposes at 215 °C according to

$$2SrO_2 \xrightarrow{\Delta T} 2SrO + O_2. \tag{A2}$$

A stoichiometric amount of SrO_2 powder has been introduced in the glass spheres, prior to evacuation, filling with ^{3}He, and sealing. Then, the cells have been placed into an oven at 300 °C to release the oxygen.

Table I lists the filling pressures (p_{He}) and the sample volumes (V) of the four glass spheres used to measure the calibration coefficient, η, that relates the average (initial) FID signal amplitude, $\langle S_{th}\rangle$, to these experimental parameters and the equilibrium nuclear polarization:

$$\langle S_{th}\rangle = \eta |P_{th}| V\, p_{He}. \tag{A3}$$

Figure 7 shows the compilation of the values of η inferred from Eq. (A3), obtained from NMR measurements performed at fixed amplifier gain on the four O_2-doped ^{3}He samples listed in Table I. Within experimental error bars, the data are consistent with a constant value of the coefficient η, which shows that potential differences in filling factors (which combine coil sensitivity and rf field inhomogeneity averaged over the sample volume) are negligible.

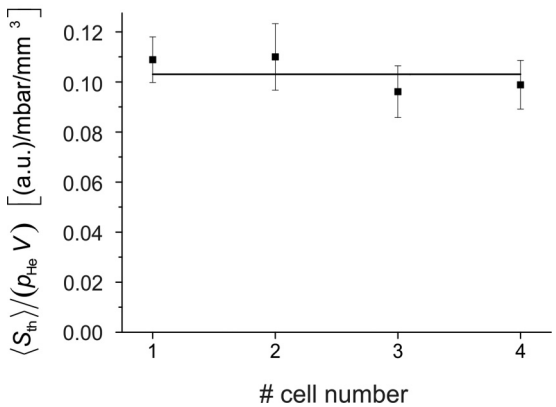

FIG. 7. Compilation of data obtained from NMR measurements performed on thermally polarized ^{3}He gas, using four O_2-doped samples listed in Table I. They yield the weighted average value of the calibration coefficient introduced in Eq. (A3): $\eta = (0.103 \pm 0.005)$[a.u.]/mbar/mm^3.

The absolute value of discharge-induced nuclear polarization, $|P_\infty|$, asymptoticaly reached in a sealed ^{3}He cell of volume V and filling pressure p_{He}, can thus be derived from the measured signal amplitude S_∞ using

$$|P_\infty| = \frac{S_\infty}{\eta V\, p_{He}}. \tag{A4}$$

APPENDIX B: CONSIDERATIONS ON ALIGNMENT-TO-ORIENTATION CONVERSION IN HELIUM

In the fields of optical spectroscopy and atomic physics, gas discharges are known as excellent media for the observation and use of unbalanced distribution of populations between energy levels, but also between magnetic sublevels. Lombardi and Pébay-Peyroula [33] showed that high-frequency capacitive discharges could be used to induce alignment in a gas, as a result of an anisotropic bombardment. Fano, Lehmann, Lombardi, and others have exhibited conditions in which the alignment could develop into orientation and proposed theoretical descriptions of the so-called alignment-to-orientation conversion processes (see [34,35] and references therein). Lombardi also proposed application of AOC in high-frequency discharges for polarization of nuclear spin of ^{3}He ground-state atoms [36,37], but we are not aware of such experiments. In the following an incomplete description of PAMP is given, in terms of selective atomic excitation by free electrons and AOC-induced nuclear polarization of ^{3}He through $2\,^3P \rightarrow 2\,^3S$ radiative decay and metastability exchange collisions.

1. Electronic excitation in the rf discharge

The time-averaged rf power dissipated into the plasma is given by the volume integral

$$P_d = \iiint \sigma |E_{rf}|^2 dV, \tag{B1}$$

where E_{rf} is the amplitude of the rf electric field and σ is the plasma conductivity given by

$$\sigma = \frac{e^2\, \bar{n}_e\, \nu_e}{m_e\left(\omega^2 + \nu_e^2\right)}. \tag{B2}$$

Here, $\bar{n}_e$ denotes the average electron density, ω is the rf field frequency, and ν_e is the electron collision frequency. The strong magnetic field affects the transverse plasma transport in the cell due to the reduction of the transverse conductivity

$\sigma_\perp$ according to

$$\sigma_\perp = \frac{\sigma}{1+\omega_c^2/\nu_e^2}, \tag{B3}$$

where $\omega_c = eB/m_e$ is the cyclotron frequency of the electron. While the transverse component of the conductivity decreases with increasing B and becomes very small for $\omega_c \gg \nu_e$, the magnetic field does not affect the longitudinal component of the conductivity $\sigma_\parallel = \sigma$. The condition $\sigma_\perp \ll \sigma_\parallel$ characterizes magnetic confinement and applies to the so-called magnetized plasmas. It is met whenever the cyclotron (or gyration) radius r_c is much smaller than the mean free path $\lambda = (\sigma_{coll} n_{He})^{-1}$ of the electrons in the gas. The elastic collision cross section of electrons in He gas is $\sigma_{coll} \approx 7 \times 10^{-16}\,\mathrm{cm}^2$ [38] at electron energies $E_e \leqslant 4$ eV. For each gas sample, the helium number density n_{He} is constant and given by the cell filling pressure p_{He} and filling temperature T_0 ($T_0 \approx 300$ K). Thus, the ratio of mean free path λ to cyclotron radius r_c weakly depends on the actual gas temperature T and essentially varies with the magnetic-field strength B according to

$$\frac{\lambda}{r_c} = \frac{\omega_c}{\nu_e} \approx 67 \frac{T}{T_0} \frac{B[\mathrm{T}]}{p_{He}[\mathrm{mbar}]}. \tag{B4}$$

In our experimental conditions ($B = 4.7$ T, $1 \leqslant p_{He}[\mathrm{mbar}] \leqslant 15$) we find that $(\omega_c/\nu_e)^2$ always exceeds 440, the base value being obtained for the highest filling pressure. The primary effect of the magnetic field is to confine electrons within a cyclotron radius (of the order of micrometers at field strength of a few tesla) and depress diffusion across the magnetic field while electrons can freely stream in the direction of B (z axis). Moreover, electrons cannot pick up energy by the transverse component of the electric field apart from the negligible amount associated with the slow transverse magnetron motion at velocity $\upsilon = E \times B/B^2$. Hence transverse momentum can only be obtained indirectly from longitudinal momentum by collisions and remains necessarily much smaller on average. Therefore, in a magnetized plasma the momentum of the exciting electrons is fairly well aligned along B.[10]

In the seminal paper by Fano and Macek [34] it is stated that the excitation of an atom or molecule by unidirectional collision in a gas leaves it generally in an anisotropic state. The collision process determines the components of the alignment tensor and orientation vector in a "collision frame" the $\hat{z}$ axis of which usually coincides with the direction of an incident particle beam. In the simplest case, e.g., an unpolarized electron beam incident on gas atoms, the experimental arrangement identifies only this $\hat{z}$ axis and has cylindrical symmetry about it. Under these circumstances, the alignment tensor has a single nonzero component (the situation met in the alignment experiment of [39], for example). The orientation vector, however, vanishes because it is an axial vector and no such quantity can be identified in a frame characterized by a single vector $\hat{z}$, unless the particles have nonzero helicity. For instance, optical pumping using circularly polarized light (incident photon beam) is the typical example of how one can directly achieve orientation in the atomic system.

In an aligned atomic system, states of different $|m_J|$ are populated unequally, while the populations in m_J and $-m_J$ are the same. In contrast, an oriented system is characterized by differing populations in the m_J and $-m_J$ states.

Electron impact excitations of atoms and in particular the total cross sections for the $1\,^1S \to 2\,^3S$ and $2\,^3P$ excitation from the ^{3}He atomic ground state as well as the $2\,^3S \to 2\,^3P$, $3\,^3P$, $3\,^3D$, and $4\,^3D$ excitations from the metastable $2\,^3S$ state of helium have been calculated by [40]. At electron energies around 4 eV (or an electron velocity $\upsilon_e = 1.2 \times 10^6$ m/s) the $2\,^3S \to 2\,^3P$ collisional excitation peaks at $\sigma(2\,^3S \to 2\,^3P) \approx 10^{-14}\,\mathrm{cm}^2$, whereas the cross sections of the other transitions are much smaller.[11]

The collisional excitation rate for this transition is given by

$$\Gamma_{2\,^3S\to 2\,^3P} = n_e(4\,\mathrm{eV})\upsilon_e \sigma(2\,^3S \to 2\,^3P). \tag{B5}$$

The electron number densities n_e at ~4 eV reach values of $n_e > 10^{10}\,\mathrm{cm}^{-3}$ in medium and strong discharge plasmas [23,42,43], which results in $\Gamma_{2\,^3S\to 2\,^3P} > 10^4 \mathrm{s}^{-1}$. For comparison, the corresponding excitation rate from the atomic ground state to the $2\,^3P$ state[12] is $\Gamma_{1\,^1S\to 2\,^3P} \approx 10^{-3}\mathrm{s}^{-1}$. Altogether, the creation rate (in $\mathrm{cm}^{-3}\,\mathrm{s}^{-1}$) of $2\,^3P$ atoms $\Gamma_{2\,^3S\to 2\,^3P} N^* + \Gamma_{1\,^1S\to 2\,^3P} N_{gs}$ is mostly set by excitations from the $2\,^3S$ state, although the proportion of ^{3}He atoms in the $2\,^3S$ state (N^*/N_{gs}) lies in the 1–10-ppm range, at most, in our operating conditions [19]. According to the semiclassical approach introduced by Seaton [44] which is known as the impact parameter method, the $2\,^3S \to 2\,^3P$ collisional excitation cross section has the interpretation that, due to the field of the atomic electron, the colliding electron ($\hat{z}$ axis) emits a photon which is subsequently absorbed by the atom in the $2\,^3S \to 2\,^3P$ transition with $\omega_{SP} = 1.16\,\mathrm{eV}/\hbar$. The electric dipole matrix element of this transition corresponds to a π transition ($\Delta m_L = 0$) which creates alignment in the excited state.

2. Alignment-to-orientation conversion

Conversion of the excited-state alignment into orientation can occur during the time between excitation and decay. As shown by Fano and Macek [34], this cannot result from internal interactions alone, but can take place if these interactions (spin-orbit coupling or hyperfine coupling, or both) are combined with the action of an external magnetic field (Zeeman energy) which introduces the necessary axial vector into the

[10]The voltage drop across the rf discharge coil [see Fig. 1(b)] causes an axial electric field (capacitively coupled discharge). Due to Faraday's law the axial magnetic field also generates an azimuthal electric field (inductively coupled discharge) which, however, is irrelevant for the gas discharge process because condition $\sigma_\perp \ll \sigma_\parallel$ is met.

[11]Cross sections for the spin-forbidden transitions $\mathrm{He}^*(2^3S) \to \mathrm{He}^*(2^1P)$, $\mathrm{He}^*(2^1S)$ can amount to $8 \times 10^{-16}\,\mathrm{cm}^2$ [41].

[12]$\Gamma_{1\,^1S\to 2\,^3P}$ can be derived from Eq. (B5), using $\sigma(1\,^1S \to 2\,^3P) \approx 5 \times 10^{-18}\,\mathrm{cm}^2$ [41], $n_e(25\,\mathrm{eV})/n_e(4\,\mathrm{eV}) \approx 10^{-4}$ [23], and $\upsilon_e(25\mathrm{eV})/\upsilon_e(4\mathrm{eV}) = 2.5$.

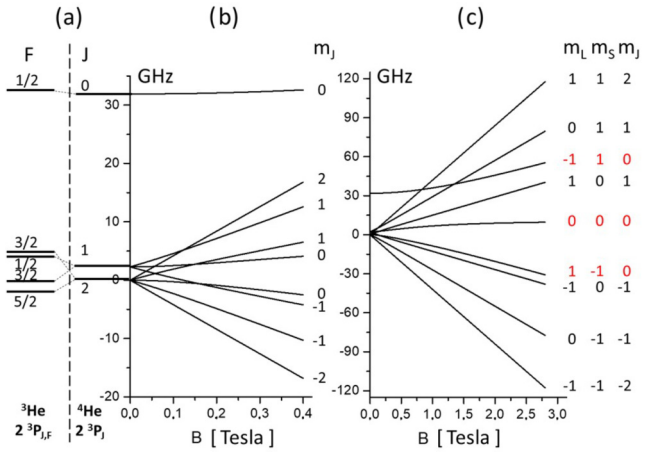

FIG. 8. (a) Level structure in zero field of the $2\,^3P$-multiplets for ^{3}He and ^{4}He (isotope shift discarded). (b) Zeeman splitting of ^{4}He states up to 0.4 T. (c) Zeeman splitting of ^{4}He states up to 3 T. On the right are shown asymptotic Paschen-Back quantum numbers. Two distinguished field regions where an increased AOC occurs are around $B \sim 0.2$ T where the $J = 2$ and 1 levels with the same m_J quantum repel each other (anticrossing) and at higher fields around $B \sim 1.1$ T where the three ($m_J = 0$) levels are involved in the high-field avoided crossing.

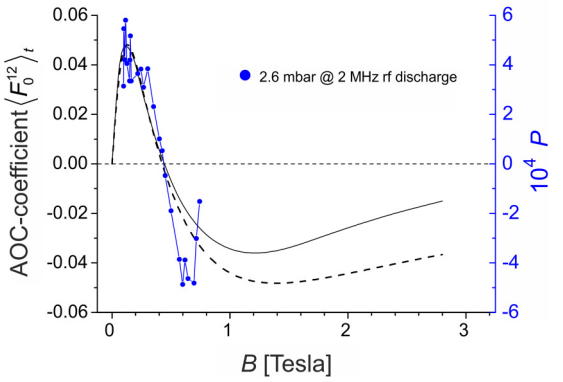

FIG. 9. Discharge nuclear polarization measured by McCall and Carver (blue data points, right vertical axis) as a function of magnetic field for a sample pressure of $p_{\mathrm{He}} \approx 2.5$ mbars [17]. For $B > 0.7$ T the drop in polarization magnitude was attributed to field inhomogeneities. Time-averaged AOC coefficient $\langle F_0^{12} \rangle_t$ (black solid line) for $2\,^3P$ levels of helium (^{4}He) vs the magnetic-field strength as calculated by Nehring [46] using the formalisms of Fano and Macek [34]. Apart from a still unknown experiment-related conversion factor these theoretical results describe the field dependence of the measured polarization values with the sign change at $B \sim 0.45$ T. The dashed line is a simplified analytical description of the field dependence of $\langle F_0^{12} \rangle_t$ according to Eq. (B8) normalized to the first peak maximum of Nehring's result.

Hamiltonian. Ignoring hyperfine terms (Hfs) for the present, the alignment-to-orientation conversion is most efficient in all cases when

$$\mu_{\mathrm{B}} B(L_z + 2S_z) \approx a\,LS, \tag{B6}$$

i.e., when the Zeeman and spin-orbit energies are comparable [35] with a being the spin-orbit coupling strength.

Quantum mechanically, this AOC process may be viewed as resulting from the mixture of the wave functions of coupled fine-structure (Fs) levels and decoupled Paschen-Back levels in the intermediate field region where states with equal m_J repel each other with opposite curvature, so called anticrossings or avoided level crossings. As an important consequence there is a redistribution of the level's eigenfunctions and therefore of the populations near the avoided crossing point.[13]

Figure 8 shows the energy diagram of the $2\,^3P_j$ sublevels of ^{4}He—which we discuss first—as a function of the magnetic-field strength. At zero field the spacings are due to the spin-orbit interaction plus a marked downshift of the $2\,^3P_1$ state by residual interaction with the $2\,^1P_1$ state. The wave functions are well described by the coupled $|LSJ, m_J\rangle$ representation. At field strength $B > 3$ T they are essentially decoupled in the $|LS, m_L, m_S, m_J\rangle$ representation. AOC occurs in the transition region between these two limiting cases where terms with the same m_J repel each other through the spin-orbit coupling and thus avoid the crossing.

Nehring [46] performed detailed numerical computations of the time-averaged AOC coefficient $\langle F_0^{12} \rangle_t$ of the $2\,^3P_j$ multiplet of ^{4}He and identified two field regions where $\langle F_0^{12} \rangle_t$ peaks, with opposite signs: at low field, around $B \sim 0.2$ T, where the $J = 2$ and 1 levels with the same m_J quantum number repel each other, and at high field, around $B \sim 1.1$ T, where $\mu_B B$ is comparable to the 30-GHz splitting between the $^3P_1$ and $^3P_0$ states. The calculated magnetic-field dependence of the time-averaged orientation of the $2\,^3P$ state of helium (following an instantaneous alignment) is shown by the black solid line in Fig. 9 (e). This line reproduces the shape of the experimental polarization curve of McCall and Carver [17] and the zero crossing.

On a more elementary basis without advanced formalism, the transient AOC effect can be described using the analytical formula of Eq. (B7) from Kemp *et al.* [35] derived for a simpler prototype case, i.e., an alkali-metal-like atom or ion (without Hfs) with s ground state and excitation into an aligned p-doublet state. If the radiative lifetime of the p state is long compared to the spin-orbit and Zeeman precession times, the magnetic-field dependence of the time-averaged fractional orientation, here denoted by $\langle q_a \rangle_t$, is given by

$$\langle q_a \rangle_t = \frac{-(a/\mu_{\mathrm{B}})B}{9/4(a/\mu_{\mathrm{B}})^2 + B^2}, \tag{B7}$$

which reaches a deep minimum of -1/3 when $\mu_{\mathrm{B}} B$ equals the doublet-splitting $(3/2)\,a$ and shows an asymptotic slope $\sim 1/B$. Applying tentatively Eq. (B7) to the $2\,^3P_J$ triplet of ^{4}He, we may set $a_1/\mu_{\mathrm{B}} = 0.11$ T and $a_2/\mu_{\mathrm{B}} = 0.73$ T to describe the low-field maximum and the high-field minimum, respectively, reported in Ref. [17]. The $\langle F_0^{12} \rangle_t$ curve apart from overall normalization and amplitudes' weighting

[13]The effects of such situations are widely spread in physics. Related to NMR, anticrossings provide the mechanism of HP transfer from an NMR silent state (singlet) to an observable state (triplet) (see, e.g., [45]).

factors is reproduced reasonably well (see Fig. 9, dashed black line) by

$$\langle F_0^{12}\rangle_t \approx |\langle q_{a_1}\rangle| - |\langle q_{a_2}\rangle|. \tag{B8}$$

Experimentally, we observe sizable nuclear polarization up to $P \sim -9\%$ at $B = 4.7\,\mathrm{T}$, a field strength that lies well beyond the high-field minimum and for which the predicted AOC coefficient does not exceed 2% (see Fig. 9). Even smaller polarization values may actually be expected for ^{3}He ground-state atoms, since the rf gas discharge plausibly induces partial atomic alignment only.

The obvious discrepancy between theoretical expectations at high field (from [46]) and our polarization measurements is a matter of investigation—in particular, also, with regard to the results of [35] on alkali-metal-like atoms: the computed coefficient describing the evolution of aligned p states into oriented ones can reach $\langle q\rangle = -33\%$ [see Eq. (B7)].

It should be noted that Nehring [46] and Kemp *et al.* [35] primarily treat an astrophysical observation that was still unexplained then, namely, the alignment and circular polarization of He lines (predominantly ^{4}He) occurring in sunspots which actually feature a magnetized plasma.

To include hyperfine coupling ($A\ I\ J$) in going to ^{3}He, additional contributions to $\langle F_0^{12}\rangle_t$ may occur when $g_J\mu_B B\ J \approx A\ I\ J$ where g_J is the Landé g factor for the J multiplet. The induced orientation process can operate through the hyperfine and electron-Zeeman couplings in a manner very similar to the purely electronic process. In ^{3}He the fine and hyperfine interaction strengths are comparable, at least for the $J = 1$ and 2 states of the $2\,^3P_j$ multiplet. The hyperfine splitting yields five states $|LSJF, m_F\rangle$ with 18 Zeeman components altogether (see Fig. 8, left-hand side). The present qualitative treatment cannot predict on a quantitative basis the presumable field dependence of the AOC-effect-induced nuclear ground-state polarization of ^{3}He including the metastability exchange mechanism. Regarding the Carver and coworkers data (see Fig. 9, blue line and dots), the inclusion of hyperfine coupling may account for the observed fine structure in the polarization curve measured around ~0.2 T. An appropriate calculation of the AOC-induced nuclear polarization of ^{3}He requires a full, field dependent diagonalization of the Fs and Hfs Hamiltonian as well as a proper treatment of the dynamics of collisional excitation and metastability exchange. This work is in progress and will be the subject of a forthcoming publication.

[1] F. D. Colegrove, L. D. Schearer, and G. K. Walters, Phys. Rev. **132**, 2561 (1963).
[2] C. Cohen-Tannoudji and A. Kastler, Progress in Optics **5**, 1 (1966).
[3] W. Happer, Rev. Mod. Phys. **44**, 169 (1972).
[4] M. Batz, Ph.D. thesis, UPMC–Paris 6 and Johannes Gutenberg–Universität Mainz, 2011.
[5] T. R. Gentile, P. J. Nacher, B. Saam, and T. G. Walker, Rev. Mod. Phys. **89**, 045004 (2017).
[6] B. S. Schlimme *et al.*, Phys. Rev. Lett. **111**, 132504 (2013).
[7] J. Krimmer *et al.*, Nucl. Instrum. Methods **648**, 35 (2011).
[8] W. Heil, K. H. Andersen, R. Cywinski, H. Humblot, C. Ritter, T. W. Roberts, and J. R. Stewart, Nucl. Instrum. Methods **485**, 551 (2002).
[9] J. R. Stewart *et al.*, Physica B **385–386**, 1142 (2006).
[10] E. Lelievre-Berna *et al.*, Meas. Sci. Technol. **21**, 055106 (2010).
[11] M. Ebert *et al.*, Lancet **347**, 1297 (1996).
[12] H. U. Kauczor, M. Ebert, K. F. Kreitner, H. Nilgens, R. Surkau, W. Heil, D. Hofmann, E. W. Otten, and M. Thelen, J. Magn. Reson. Imaging **7**, 538 (1997).
[13] A. Nikiel, P. Blümler, W. Heil, M. Hehn, S. Karpuk, A. Maul, E. Otten, L. M. Schreiber, and M. Terekhov, Eur. Phys. J. D **68**, 330 (2014).
[14] L. D. Schearer, F. D. Colegrove, and G. K. Walters, Rev. Sci. Instrum. **34**, 1363 (1963).
[15] H. C. Koch *et al.*, Eur. Phys. J. D **69**, 262 (2015).
[16] R. L. Gamblin and T. R. Carver, Phys. Rev. **138**, A946 (1965).
[17] G. H. McCall and T. R. Carver, Phys. Rev. Lett. **19**, 485 (1967).
[18] A. Nikiel, T. Palasz, M. Suchanek, M. Abboud, A. Sinatra, Z. Olejniczak, T. Dohnalik, G. Tastevin, and P.-J. Nacher, Eur. Phys. J.-Special Topics **144**, 255 (2007).
[19] A. Nikiel-Osuchowska, G. Collier, B. Glowacz, T. Palasz, Z. Olejniczak, W. P. Weglarz, G. Tastevin, P.-J. Nacher, and T. Dohnalik, Eur. Phys. J. D **67**, 200 (2013).
[20] M. Abboud, A. Sinatra, G. Tastevin, P. J. Nacher, and X. Maitre, Laser Physics **15**, 475 (2005).
[21] M. A. Lieberman and A. J. Lichtenberg, *Principles of Plasma Discharges and Material Processing*, 2nd ed. (Wiley, New York, 2005).
[22] C. Beneking, J. Appl. Phys. **68**, 4461 (1990).
[23] V. A. Godyak, R. B. Piejak, and B. M. Alexandrovich, Plasma Sources Sci. Technol. **1**, 36 (1992).
[24] T. Dohnalik, A. Nikiel, T. Palasz, M. Suchanek, G. Collier, M. Grenczuk, B. Glowacz, and Z. Olejniczak, Eur. Phys. J.: Appl. Phys. **54**, 20802 (2011).
[25] J. S. Boisvert, N. Sadeghi, J. Margot, and F. Massines, J. Appl. Phys. **121**, 043302 (2017).
[26] A. Maul, P. Blümler, W. Heil, A. Nikiel, E. Otten, A. Petrich, and T. Schmidt, Rev. Sci. Instrum. **87**, 015103 (2016).
[27] E. Stoltz, M. Meyerhoff, N. Bigelow, M. Leduc, P.-J. Nacher, and G. Tastevin, Appl. Phys. B-Lasers Optics **63**, 629 (1996).
[28] V. Lefevre-Seguin and M. Leduc, J. Phys. B **10**, 2157 (1977).
[29] T. Xia, S. W. Morgan, Y. Y. Jau, and W. Happer, Phys. Rev. A **81**, 033419 (2010).
[30] E. Courtade, F. Marion, P. Nacher, G. Tastevin, K. Kiersnowski, and T. Dohnalik, Eur. Phys. J. D **21**, 25 (2002).
[31] P. J. Mohr, B. N. Taylor, and D. B. Newell, Rev. Mod. Phys. **84**, 1527 (2012).
[32] B. Saam, W. Happer, and H. Middleton, Phys. Rev. A **52**, 862 (1995).
[33] M. Lombardi and J. C. Pébay-Peyroula, Compt. Rend. Hebd. Sean. Acad. Sci. **261**, 1485 (1965).
[34] U. Fano and J. H. Macek, Rev. Mod. Phys. **45**, 553 (1973).
[35] J. C. Kemp, J. H. Macek, and F. W. Nehring, Astrophys. J. **278**, 863 (1984).
[36] M. Lombardi and M. Giroud, Compt. Rend. Hebd. Sean. Acad. Sci. Ser. B **266**, 60 (1968).
[37] M. Lombardi, J. Phys. **30**, 631 (1969).

[38] M. J. Brunger, S. J. Buckman, L. J. Allen, I. E. McCarthy, and K. Ratnavelu, J. Phys. B **25**, 1823 (1992).
[39] T. Hadeishi and C. H. Liu, Phys. Rev. Lett. **19**, 211 (1967).
[40] B. L. Moiseiwitsch and S. J. Smith, Rev. Mod. Phys. **40**, 238 (1968).
[41] W. C. Fon, K. A. Berrington, P. G. Burke, and A. E. Kingston, J. Phys. B **14**, 2921 (1981).
[42] G. Dilecce, M. Capitelli, and S. Debenedictis, J. Appl. Phys. **69**, 121 (1991).
[43] K. Dzierzega, K. Musiol, E. C. Benck, and J. R. Roberts, J. Appl. Phys. **80**, 3196 (1996).
[44] M. J. Seaton, Proc. Phys. Soc. London **79**, 1105 (1962).
[45] L. Buljubasich, M. B. Franzoni, H. W. Spiess, and K. Münnemann, J. Magn. Reson. **219**, 33 (2012).
[46] F. W. Nehring, Ph.D. thesis, University of Nebraska, 1979.